Molecular Cell
Article

Structural Basis of Assembly Chaperone-Mediated snRNP Formation

Clemens Grimm,[1,5,*] Ashwin Chari,[1,3,5] Jann-Patrick Pelz,[1] Jochen Kuper,[2] Caroline Kisker,[2] Kay Diederichs,[4] Holger Stark,[3] Hermann Schindelin,[2] and Utz Fischer[1,2,*]

[1]Department of Biochemistry, Theodor Boveri Institute, University of Wuerzburg, Am Hubland, 97074 Wuerzburg, Germany
[2]Rudolf-Virchow-Zentrum, DFG Research Centre for Experimental Medicine, University of Wuerzburg, Josef-Schneider-Strasse 2, Haus D15, 97080 Wuerzburg, Germany
[3]Max Planck Institute for Biophysical Chemistry, Am Faßberg 11, 37077 Goettingen, Germany
[4]Protein Crystallography and Molecular Bioinformatics, University of Konstanz, 78457 Konstanz, Germany
[5]These authors contributed equally to this work
*Correspondence: clemens.grimm@uni-wuerzburg.de (C.G.), utz.fischer@biozentrum.uni-wuerzburg.de (U.F.)
http://dx.doi.org/10.1016/j.molcel.2012.12.009

SUMMARY

Small nuclear ribonucleoproteins (snRNPs) represent key constituents of major and minor spliceosomes. snRNPs contain a common core, composed of seven Sm proteins bound to snRNA, which forms in a stepwise and factor-mediated reaction. The assembly chaperone pICln initially mediates the formation of an otherwise unstable pentameric Sm protein unit. This so-called 6S complex docks subsequently onto the SMN complex, which removes pICln and enables the transfer of pre-assembled Sm proteins onto snRNA. X-ray crystallography and electron microscopy was used to investigate the structural basis of snRNP assembly. The 6S complex structure identifies pICln as an Sm protein mimic, which enables the topological organization of the Sm pentamer in a closed ring. A second structure of 6S bound to the SMN complex components SMN and Gemin2 uncovers a plausible mechanism of pICln elimination and Sm protein activation for snRNA binding. Our studies reveal how assembly factors facilitate formation of RNA-protein complexes in vivo.

INTRODUCTION

Macromolecular complexes facilitate an assortment of biological tasks in cells of all organisms (Alberts, 1998; Hartwell et al., 1999). These complexes are constantly assembled de novo and with high accuracy from individual subunits amidst high concentrations of biological macromolecules present in living cells (Ellis, 2001). The assembly of macromolecular complexes in vivo is often aided by a heterogeneous group of proteins referred to as assembly chaperones. These factors promote the formation of higher-order subcomplexes, while simultaneously preventing noncognate interactions (Chari and Fischer, 2010; Ellis, 2006). A frequent consequence of assembly chaperone action is the formation of kinetically trapped intermediates, which are prevented from proceeding in the assembly pathway. Hence, additional *trans*-acting factors are essential to release the preassembled subcomplexes from their stalled state and allow their joining to functional units.

A group of macromolecular complexes that follows the assembly principles summarized above include the Sm class of small nuclear ribonucleoproteins (snRNPs). These particles represent the major building blocks of the major and minor spliceosome and thus constitute essential factors in the splicing of all cellular pre-mRNAs (Tarn and Steitz, 1997; Wahl et al., 2009). Despite the functional differences between individual spliceosomal snRNPs, they all share a similar architecture. They consist of a name-giving snRNA and a variable set of snRNP-specific proteins with defined functions in splicing. In addition, all snRNPs contain seven evolutionarily related Sm proteins termed B/B′, D1, D2, D3, E, F and G (B′ is a splice variant of B) that encircle a single-stranded region of the snRNA (Sm site) to form a toroidal Sm core domain (Leung et al., 2011; Pomeranz Krummel et al., 2009; Weber et al., 2010). The "Sm" fold of Sm proteins, consisting of an N-terminal α helix followed by a strongly bent five-stranded antiparallel β sheet, mediates the formation of this structure (Kambach et al., 1999). The β4 strand of one Sm protein connects to a β5 strand of an adjacent Sm protein, resulting in the formation a continuous, intermolecular β sheet. This interaction principle between individual Sm proteins is repeated in the sequence SmE-SmG-SmD3-SmB-SmD1-SmD2-SmF (from the first to the seventh nucleotide of the Sm site, respectively) to form the toroidal Sm core domain.

In vitro studies revealed that Sm proteins form distinct hetero-oligomeric building blocks composed of SmD1/D2, SmD3/B, and SmE/F/G. While none of these oligomers are capable of interacting with each other in the absence of snRNA, SmD1/D2, and SmE/F/G initially cooperatively associate with the Sm site to form a "subcore" structure (Raker et al., 1996). This intermediate matures into the Sm core upon addition of the SmD3/B heterodimer. In contrast to the spontaneous assembly observed in vitro, formation of the Sm core domain in vivo depends on a surprisingly large number of assisting factors (Chari et al., 2009; Yong et al., 2004). These factors act in the context of the biogenesis cycle of snRNPs, which involves the initial nuclear export of m^7G-capped snRNA, the assembly of the snRNP in the cytoplasm and its subsequent import into the nucleus (Fischer et al., 2011). Within this cycle, the PRMT5 complex

initially sequesters the Sm proteins in the cytoplasm and modifies distinct arginine residues in the C-terminal tails of SmB/B′, SmD1, and SmD3 to symmetric dimethylarginine (sDMA) (Friesen et al., 2001b; Meister et al., 2001b). In addition, the pICln subunit functions as an assembly chaperone for Sm proteins (Chari et al., 2008). It tethers the hetero-oligomers SmD1/D2 and SmE/F/G into a ring-shaped 6S complex that dissociates from the PRMT5 complex. In this state, Sm protein binding to snRNA is inhibited as a result of a steric occlusion of the central cavity, which prevents RNA from gaining access to its binding site (Leung et al., 2011; Pomeranz Krummel et al., 2009; Weber et al., 2010).

Additional *trans*-acting factors are required to allow the release of Sm proteins from their kinetically trapped state and the assembly reaction to proceed. These factors are united in the SMN complex, which consists of the survival motor neuron (SMN) protein, mutated in spinal muscular atrophy, and eight other proteins referred to as Gemin2–Gemin8 and unrip (Gubitz et al., 2004; Meister et al., 2001a; Pellizzoni et al., 2002). The SMN complex acts as a catalyst of snRNP formation by releasing the Sm proteins in the 6S complex (Fisher et al., 1985) from the pICln-imposed kinetic trap and transferring the Sm proteins onto snRNAs (Chari et al., 2008). The core machinery mediating snRNP assembly is evolutionarily and functionally conserved in metazoans (Kroiss et al., 2008).

Structural studies of Sm protein hetero-oligomers and even assembled snRNPs have yielded detailed insights into the architecture of snRNP cores (Kambach et al., 1999; Leung et al., 2011; Pomeranz Krummel et al., 2009; Weber et al., 2010). In addition, the structure of a complex composed of the Sm proteins D1, D2, E, F, and G bound to Gemin2 and a short fragment of SMN has recently been reported (Zhang et al., 2011). This complex provided information on Sm protein transfer onto snRNA, which represents a late phase of the assembly process. In contrast, structural insights into the early, assembly chaperone-dominated phase of snRNP assembly are entirely lacking. Hence, it is neither understood how pICln ties together the hetero-oligomers SmD1/D2 and SmE/F/G into the 6S complex even though they have little affinity for each other in the absence of snRNA, nor is it clear how the SMN complex resolves the kinetic trap imposed by pICln to allow Sm protein transfer onto snRNA. To address these questions, we have solved the crystal structures of two assembly intermediates: the 6S complex and a stalled Sm protein transfer intermediate composed of the 6S complex and the SMN complex subunits SMN and Gemin2 (termed 8S complex). The structures establish that pICln mimics an Sm fold, which enables Sm proteins to interact with each other even in the absence of snRNA. A negative-stain electron microscopy (EM) reconstruction of the 8S complex additionally allowed us to locate flexible, albeit functionally relevant elements. Furthermore, among the 20 molecules in the asymmetric unit of the 8S complex crystals we were able to observe considerable conformational variability that culminates at the interface between pICln and SmG. These findings suggest that the elimination of pICln from the 6S complex is initiated by a ring opening at this position, driven by the molecule's conformational flexibility and the stabilization of an open-ring transition state by the SMN-complex.

RESULTS

Crystal Structure of the 6S Assembly Intermediate at 1.9 Å Resolution

To elucidate the structural basis of pICln's role as an assembly chaperone, we screened for a 6S complex with good crystallization behavior. These efforts included mutation of surface residues for surface entropy reduction (SER) (Derewenda and Vekilov, 2006) and were guided by the prior knowledge of the 8S crystal structure (see below). A chimeric complex composed of human SmD1/D2 and SmE/F/G and a truncated form of *Drosophila melanogaster* pICln lacking amino acids 90–125 and carrying a H144A mutation yielded crystals that diffracted to 1.9 Å. A similar complex comprising exclusively components of human origin turned out to be significantly less stable (data not shown). The structure was solved and refined to an R factor/free R factor of 0.18/0.22 (Table 1) as described in Experimental Procedures.

In the crystal structure, the 6S complex adopts an elliptical, toroidal structure with dimensions of 72 Å along the longer pICln-SmF axis and 65 Å along the shorter SmD1-SmE axis (Figure 1A). Distinct topological features can be discerned on the pICln/Sm ring surface: (1) a flat face in the region where the N-terminal helices of Sm proteins and the C-terminal helix of pICln reside, (2) a tapered face harboring the L4 loops of the Sm proteins and the L3 loop of pICln, and (3) the surface of the torus' central cavity (see Figure 1A for an overview of the structure and Figure 1B for an overview of pICln's fold). The crystal structure reveals that Sm proteins are organized in an identical sequence in the 6S complex as in the snRNP core, with pICln assuming the position of SmD3/B (in the sequence SmE-SmG-pICln-SmD1-SmD2-SmF) and roughly occupying the angular space of 1 ½ Sm proteins. Consequently, the 6S ring appears to be narrower and slightly elongated in comparison to the mature Sm core domain of snRNPs (Leung et al., 2011; Pomeranz Krummel et al., 2009; Weber et al., 2010), even though the global dimensions are very similar (Figure 1C).

Within the 6S complex, the Sm proteins interact with each other through antiparallel pairing of the β strands of their Sm folds. This interaction mode is identical to canonical Sm contacts within assembled Sm cores (Kambach et al., 1999). pICln, in contrast, does not adopt an Sm fold but rather displays an extended pleckstrin homology (PH) topology (Figure 1B). Here, the seven antiparallel β strands (β1–β7) of a conventional PH domain are appended by an additional N-terminal β strand (termed β0), which is connected to β1 by an elongated loop (L0) and lies adjacent to β4 in an antiparallel orientation (Figure 1B). Nevertheless, pICln contacts SmD1 in a similar mode as observed between Sm proteins (Figure 1A). β5 of pICln's extended PH domain interacts with β4 of SmD1 to form an antiparallel β pair. Interestingly, a comparable contact cannot be established between pICln and SmF, which likewise exposes its β4 strand in the SmE/F/G heterotrimer (see Figure S1 available online). The short β0 strand of pICln, which is located on the opposite side of the extended PH domain, establishes the contact to SmG in the 6S complex. Remarkably, β0 pairs in a parallel, rather than an antiparallel orientation with strand β5 of SmG to establish a continuous intermolecular β sheet (Figure 1A).

Table 1. Crystallographic Data Collection and Refinement Statistics

	6S Crystal	8S Crystal
Data Collection		
Wavelength (Å)	0.9393	0.9762
Space group	C2	$P2_1$
Cell dimensions: a, b, c (Å)	180.67, 65.22, 99.22	150.93, 356.81, 230.75
Cell dimensions: α, β, γ (°)	90.0, 92.5, 90.0	90.0, 97.3, 90.0
Number molecules in asymmetric unit	2	20
Resolution (Å)	49.6–1.9 (2.01–1.9)	59.5–3.1
Ellipsoidal truncation along a*, b*, c* (Å)	–	3.1, 3.8, 4.0
Unique reflections	88,058	281,563
Rsym (%)	4.4 (58.2)	13.9 (50.5)[a], 20.0 (92.8)[b]
Mean I/σ(I)	14.3 (1.84)	5.8 (2.31)[a], 4.6 (1.35)[b]
Completeness (%)	96.2 (96.2)	98.9 (96.7)[a], 64.6 (5.8)[b]
Redundancy	2.69 (2.71)	3.9 (3.9)[a], 3.9 (3.9)[b]
Refinement		
Resolution (Å)	49.6–1.9	59.4–3.1
Number of reflections	88,058	281,563
R/R_{free}	0.178/0.221	0.232/0.256
Number of atoms: protein	8,140	121,940
Number of atoms: ligand/ion	31	50
Number of atoms: water	372	0
Rmsd: bond lengths (Å)	0.012	0.010
Rmsd: bond angles (°)	1.520	1.290
Ramachandran: favored, allowed, outliers (%)	98.3, 1.8, 0.0	92.4, 5.2, 2.4
PDB ID code	4F7U	4F77

[a]For resolution range of 60–4.0 Å, the number in parentheses corresponds to the highest-resolution shell of 4.23–4.0 Å.
[b]For resolution range of 60–3.1 Å, without ellipsoidal truncation, the number in parentheses corresponds to the highest-resolution shell of 3.29–3.10 Å.

In addition to these interactions dominated by hydrogen bonds, a strong charge complementarity between pICln and the Sm proteins of the 6S complex is evident. Poisson-Boltzmann calculations revealed that the positive electrostatic potential of the Sm proteins and the pronounced negative potential of pICln are mostly located on the molecular surface that lines the central cavity of the complex (Figure 1D). The dipole vector of pICln adopts a radial orientation with respect to its position in the pICln/Sm ring and its negative pole would point toward the central cavity (Figure 1D, lower left image). It therefore appears ideally aligned to foster an accurate preorientation of the chaperone in the early phase of binding.

Thus, two features of pICln enable formation of the 6S complex. Its extended PH fold allows the formation of a continuous β sheet that spans all six complex members. Furthermore, the charge complementary between pICln and the inner surface of the Sm protein pentamer is likely to contribute to the stability of 6S.

Crystal Structure of a Stalled Sm Protein Transfer Intermediate

In the next step of snRNP assembly, the SMN complex accepts the preformed Sm pentamer of the 6S complex and simultaneously dissociates it from the assembly chaperone pICln (Chari et al., 2008). To gain structural insights into this reaction a stalled intermediate, termed 8S complex, was reconstituted and crystallized. It consists of the human hetero-oligomers SmD1/D2 and SmE/F/G, as well as *Drosophila melanogaster* pICln (residues 1–180), SMN (residues 1–122) and full-length Gemin2 (residues 1–245). The crystals contained 20 molecules of the 8S complex in the asymmetric unit and displayed strongly anisotropic diffraction, with resolution limits along the a, b, and c axes of 3.1 Å, 3.8 Å, and 4.0 Å, respectively. The structure was solved by molecular replacement as described in the Experimental Procedures and refined with NCS restraints to an R factor/free R factor of 0.23/0.26. See Table 1 for complete data collection and refinement statistics. The high-resolution 6S structure was used as a reference model in the late refinement phase. For the final rounds of refinement NCS and reference model restraints were released for divergent parts of the model.

Superimposition of the 6S model onto the 8S crystal structure revealed that the Sm proteins and pICln adopt a similar ring-shaped arrangement in both complexes with a root-mean-square deviation (rmsd) of only 0.57 Å (see Table S1). The major distinction between both structures is therefore the Gemin2/SMN unit, which is located on the tapered face of the pICln/Sm ring. A hallmark of the Gemin2 structure is a C-terminal domain (CTD, amino acids 73–245), consisting of an exclusively helical fold that comprises seven α and two 3_{10} helices (see Figure 2A for the 8S structure, Figure 2B for the Gemin2/SMN unit, and Figure S2 for a comparison with the structure of the late intermediate [Zhang et al., 2011] Protein Data Bank [PDB] ID code 3S6N [gray overlay]). Gemin2 binds to a cleft between SmD1 and SmD2 and forms extensive contacts to the tapered face of the pICln/Sm ring. From this location the polypeptide chain runs along the SmD2-SmF interface onto the flat face, where it connects to helix α1. Gemin2 embraces the pICln/Sm ring on both faces by this extension and thereby specifically contacts both SmF and SmE by its only β strand and helix α1, respectively. Whereas Gemin2 was readily visible in our model, only the N terminus of SMN (amino acids 8–24) could be assigned to electron density. It forms a single α helix that contacts Gemin2 in its CTD, thus confirming prior biochemical and structural studies (Bühler et al., 1999; Zhang et al., 2011).

The X-ray structure of the 8S complex revealed how SMN and Gemin2 contact the 6S assembly intermediate. However, important elements of the 8S complex including the Tudor domain of SMN, which binds to symmetrically methylated arginine and is mutated in SMA patients (Brahms et al., 2001; Bühler et al., 1999; Friesen et al., 2001a), as well as the L5 loop of pICln, which harbors a large cluster of acidic residues (Figure S4; see also Figure 1D) could not be traced in the electron density. Notably, next

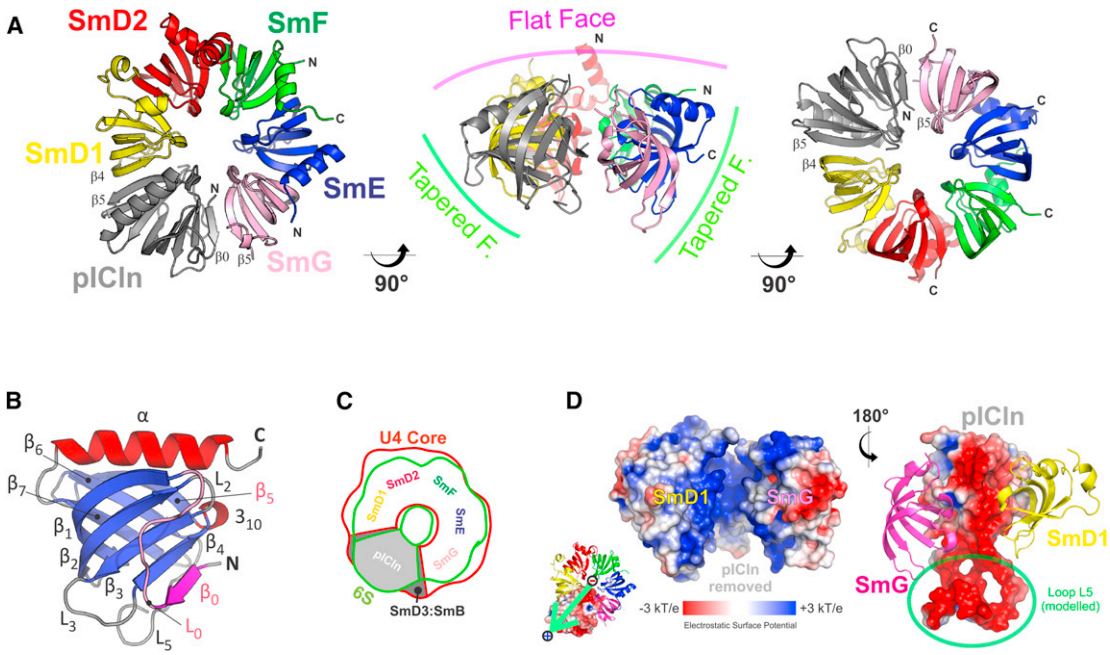

Figure 1. Structure of the 6S Complex and the Assembly Chaperone pICln

(A) Overall view of the 6S model (PDB ID code 4F7U) from three directions in ribbon representation. The left view is seen from the flat face of 6S, the right view from its tapered face. N and C termini of the individual subunits are indicated. The color code for individual proteins is used throughout the manuscript.

(B) The pICln model from the 6S structure in ribbon representation. α helices are shown in red, β strands in blue, and loops and connecting regions in gray. Strand β0 and the connecting loop L0 are highlighted in magenta and pink, respectively.

(C) Comparison of overall dimensions of the U4 core crystal structure (PDB ID code 2Y9A, contoured in red) with the 6S crystal structure (contoured in green). The positions of the individual subunits are indicated. A gray slice symbolizes the space occupied by SmD3/B and pICln, respectively.

(D) Electrostatic potential mapped onto the molecular surface of 6S. pICln (right) was removed from the ring (left) and rotated by 180°. For orientation, the two neighboring Sm proteins are shown in ribbon representation. Poisson-Boltzmann calculations were performed separately for the two resulting parts of the 6S complex (Sm pentamer and pICln). For these calculations, the pICln cover loop was modeled according to the EM density (see Figure 3) and the existing NMR structure (PDB ID code 1ZYI). The lower left image indicates the direction of pICln's dipole moment (green arrow).

See also Figure S1.

to the ring's central cavity some density was visible at low resolution and low contour levels that could not be interpreted by discrete atomic modeling (Figure S3A).

An EM 3D Reconstruction Localizes the Tudor Domain of SMN and a Cover Loop of pICln

To position those elements of the 8S complex that could not be traced in the crystallographic electron density, single-particle negative-stain electron microscopy was employed. For these studies, we utilized an 8S complex containing full-length pICln instead of the truncated version utilized for the crystallographic studies. To stabilize the 8S complex for EM analysis and to restrict the conformational mobility of the subunits we intended to visualize, this particle was subjected to GraFix (Kastner et al., 2008). The structure was reconstructed and refined as described in the Experimental Procedures. Reprojections of the obtained EM structure correspond well to their respective class averages obtained by the initial reference-free 2D classification (Figure 3A).

The 3D reconstruction revealed all the structural features present in the X-ray structure, plus some additional prominent density elements. To interpret the EM structure, we manually docked a single molecule of the 8S crystal structure (Figure 3B). The additional EM density was observed on the tapered face of the pICln/Sm ring directly adjacent to the SMN-Gemin2 CTD density of the X-ray structure, lying partially above the pICln/Sm ring's central cavity. The enclosed volume of this extra density would be sufficient in size to accommodate prominent features such as the Tudor domain of SMN and the loop connecting strands β6 and β7 of pICln's extended PH-like domain.

To interpret this additional EM density and assign individual parts to the abovementioned prominent features of the 8S molecule (Tudor domain and pICln's L5 loop), we constructed individual deletion mutants (Figure 3C). Reconstruction of an 8S complex harboring a deletion of pICln's L5 loop (Figure 3C, 8SΔcover) yields a clear, albeit truncated density additional to the elements resolved in the crystal structure on the tapered face of the pICln-Sm ring. We therefore assign this part of the additional EM density to the Tudor domain of SMN (Figures 3B and 3C, orange density). The Tudor domain filtered to the resolution of our 8S complex EM structure would fit the shape of the assigned density and lies on top of the tapered face of the 8S complex next to the tip of loop L5 from SmD1. Of note, the C-terminal tail of SmD1, which can specifically bind to SMN's

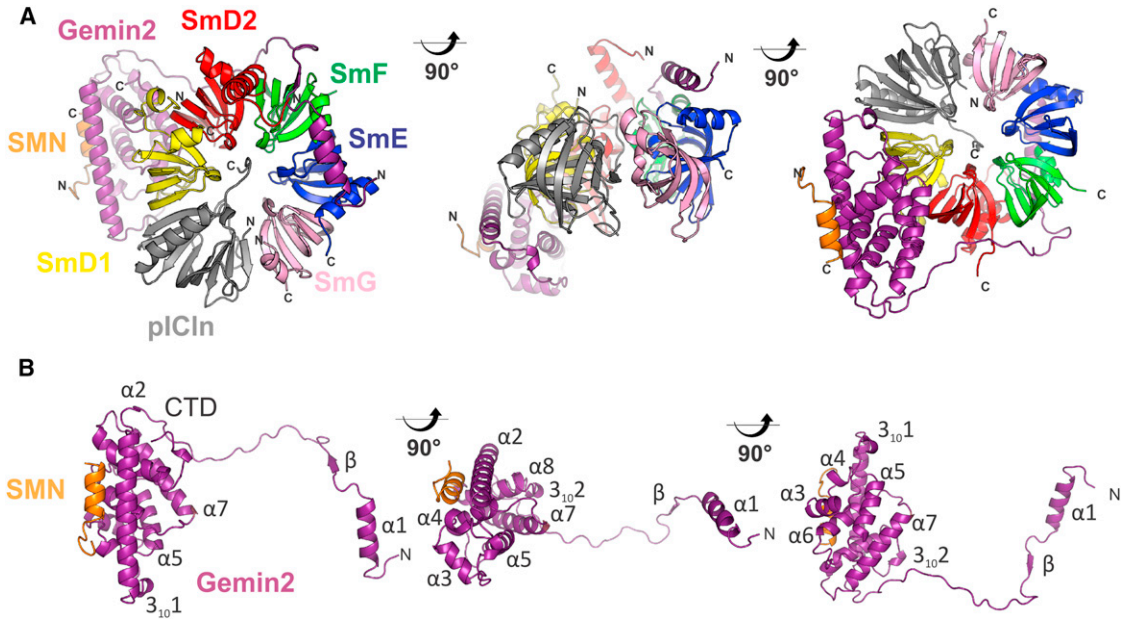

Figure 2. Structure of the 8S Complex and the Assembly Factors SMN and Gemin2

(A) Overall structure of the 8S complex (PDB ID code 4F77) viewed from the flat face of the ring (left), along the ring plane (middle), and the tapered face (right). The respective N and C termini are labeled. The subunits are color-coded as in Figure 1, Gemin2 and SMN are shown in purple and orange, respectively.

(B) Three views similar to (A); however, the pICln/Sm ring had been removed to provide a clear view of the SMN/Gemin2 moiety.

See also Figure S2.

Tudor domain in vitro, lies on the opposite, flat face of the 8S complex.

The EM density element, which disappears in the 8SΔcover structure is consequently attributed to the pICln L5 loop (Figures 3B and 3C, gray density). The extended L5 loop of pICln constricts the central cavity of the pICln/Sm ring on the tapered face, adjacent to the Gemin2 CTD. It was hence termed "cover loop." Molecular dynamics (MD) simulations further confirm the localization of the cover loop as well as the SmD2 L2 loop at this position (see Figure S5). Direct assignment of the cover loop by EM, by truncation of the Tudor domain only in the 8S complex failed (Figure 3C, 8SΔTudor). Under these circumstances, the EM reconstruction yields no density elements additional to those resolved in the crystal structure. This observation, while confirming the placement of both the Tudor domain and the pICln cover loop on the tapered face of the pICln/Sm ring, makes it likely that the cover loop, which is poorly conserved among orthologs of pICln (Figure S4) and contains no confidently predictable secondary structure elements, is conformationally mobile. In the absence of any defined specific interaction the cover loop is presumably confined to its position by virtue of the Tudor domain.

Thus, the combination of EM reconstruction, deletion engineering and MD simulation, has enabled us to locate the mobile cover loop of pICln and the Tudor domain of SMN on the tapered face of the 6S ring. Notably, the placement of these two domains on the tapered face is additionally well supported by the residual, low-resolution 2Fo-Fc and positive Fo-Fc electron density, which lies precisely in this region of the molecule (Figure S3A; compare Figure S3B) and is also in good agreement with the localization of the traceable ends of the cover loop on the molecular surface (Figure S3C).

Structure-Based Insight into the Mechanism of the snRNP Assembly Reaction

We had previously hypothesized that binding of the SMN complex induces conformational changes in the 6S complex, which leads to the destabilization of pICln's interactions with Sm proteins and its release from the ring (Chari et al., 2008). To substantiate this hypothesis, the contacts of pICln with SmD1 and SmG, respectively, were initially examined in greater detail. The interface of pICln to SmD1 is very similar to canonical Sm-Sm contacts in its biophysical nature, topology, and stability (Figure 4A; see the Supplemental Information for a detailed description). In contrast, the interface to SmG is distinctly divergent, formed by a parallel rather than an antiparallel β strand pair, which involves β5 of SmG (residues 68–70) and β0 of pICln (residues 2–4). In close vicinity, two determinants add to the stability of this β strand pair: (1) a water-mediated backbone-backbone contact between Ile4 of pICln and Ala72 of SmG at the ring periphery and (2) proximal to the central cavity, an extended H bond network around pICln's N-terminal amino group and another water molecule (Figure 4B). The remaining interface is established by van der Waals interactions that involve two methionine residues and two distinct hydrophobic pockets (Figure 4C). The first hydrophobic pocket resides on pICln (residues Ile4, Val81, and Trp83) and binds Met69 of SmG, whereas the second hydrophobic pocket is located on SmG (residues Leu9, Leu40, Ile67, and Leu70) and binds Met1 of pICln. As a consequence, both proteins interlock in a finger-joint fashion (Figure 4C). The

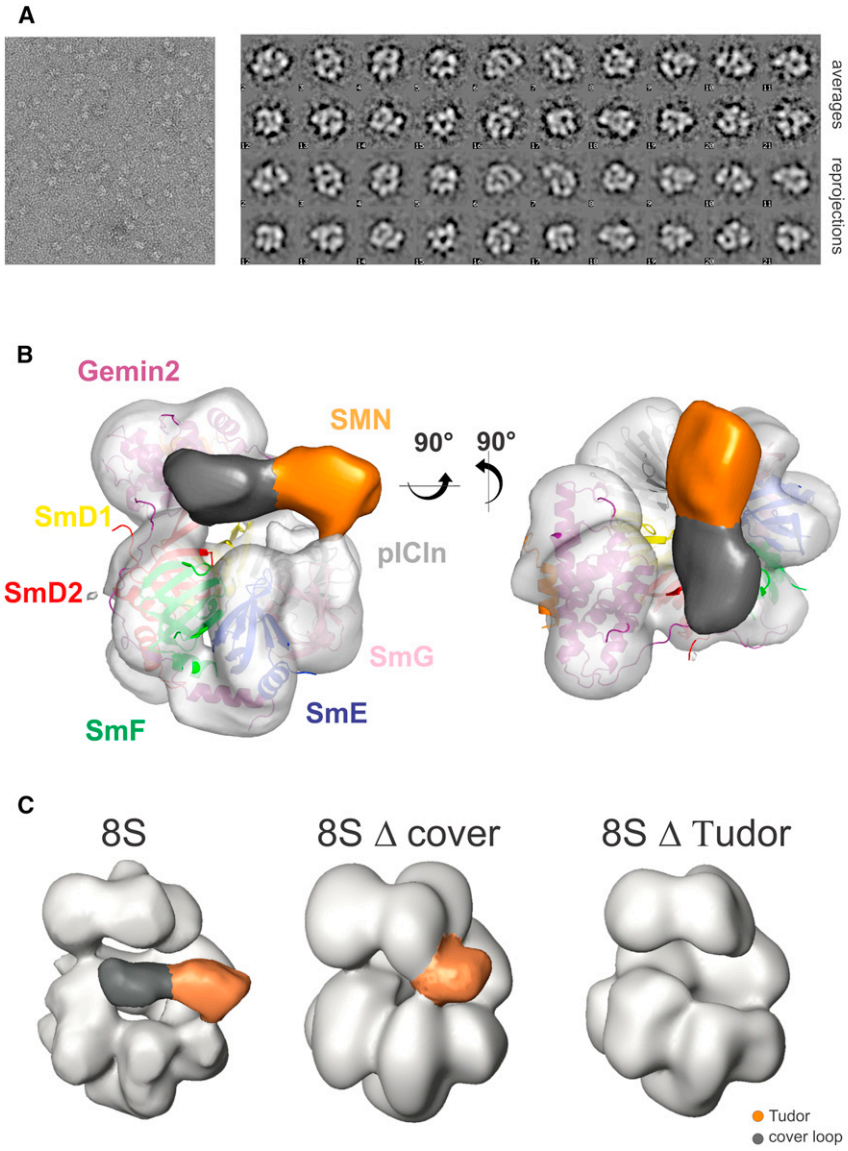

Figure 3. 3D EM Reconstruction of the 8S Complex

(A) Representative raw negative-stain image (left panel), class averages of the 8S complex (upper two rows), and reprojections of the EM reconstruction (bottom two rows).

(B) Representation of the 8S complex EM reconstruction (EMDB ID code 2102) with the fitted crystallographic model. The extra density assigned to the pICln cover loop and the SMN Tudor domains are colored according to Figure 2, in gray and orange, respectively.

(C) 3D EM reconstruction of a deletion mutant lacking the cover loop (middle), a deletion mutant lacking the tudor domain (right), and the original 8S complex for comparison (left). Note that differences in connectivities in the EM reconstructions reflect the different resolutions of the reconstruction.

See also Figure S3.

interaction surface between pICln and SmG is therefore dominated by backbone-backbone contacts and hydrophobic interactions allowing a high degree of sequence variation. This is consistent with a low evolutionary sequence conservation of pICln's interface with SmG; in contrast, the interface with SmD1 that determines the order of Sm proteins in the 6S ring is much more conserved (Figures 4D and S4). Importantly, the contact area between pICln and SmG encompasses only 450–550 Å^2 and is hence significantly smaller than all other intermolecular contacts within the pICln/Sm ring (Figure 4E). Thus, these considerations reveal a predetermined breaking point of the 6S complex between pICln and SmG.

Next, we investigated whether conformational changes occur once the SMN/Gemin2 dimer docks onto the 6S complex. Pro194 is positioned at the tip of helix α7 in Gemin2, and we noted that this residue inserts deeply into a cleft between SmD1 and SmD2 in the 8S complex (Figure 5A). SmD1-Asn24 rearranges from the surface of the 6S complex to an inward position pointing toward the central cavity of the 8S complex to accommodate Gemin2-Pro194 and the preceding amino acids in helix α1. This conformational change is necessary for Gemin2 binding as otherwise a clash would be produced (Figure 5A, indicated in red). As a consequence, SmD1-Glu18 and SmD1-Arg66 also move toward the central cavity, which is only possible by breaking two hydrogen bonds and a salt bridge between SmD1-Arg66 and SmD2-Glu72. Finally, SmD2-Asn48 collapses toward the hydrophobic core of the protein and SmD1 Arg66, which previously occupied this space, moves the L3 loop of SmD2 and the neighboring Arg47 by 3.5 Å in direction of the central cavity. Thus, Gemin2 binding to the outer face of 6S triggers a series of side chain rearrangements that propagate into the central cavity of the ring.

In addition to the altered side-chain conformations described above, we noted an intrinsic flexibility of the pICln/Sm ring by inspection of the set of 20 8S complexes present in the asymmetric unit of the crystal for conformational differences (Figure 5B). While most parts of the 8S complex appear to be conformationally rigid, a region of pronounced flexibility could be identified at the pICln-SmG interface, i.e., the postulated predetermined breaking point of the 6S ring (Figure 5B). This flexibility is also mirrored in the pronounced variation of the pICln-SmG contact area (Figure 4E). Strikingly, a movement mainly perpendicular to the ring plane aptly describes the conformational variation among the 20 molecules at this position.

We obtained additional insight into the motional dynamics of snRNP assembly from MD simulations of the 6S and 8S

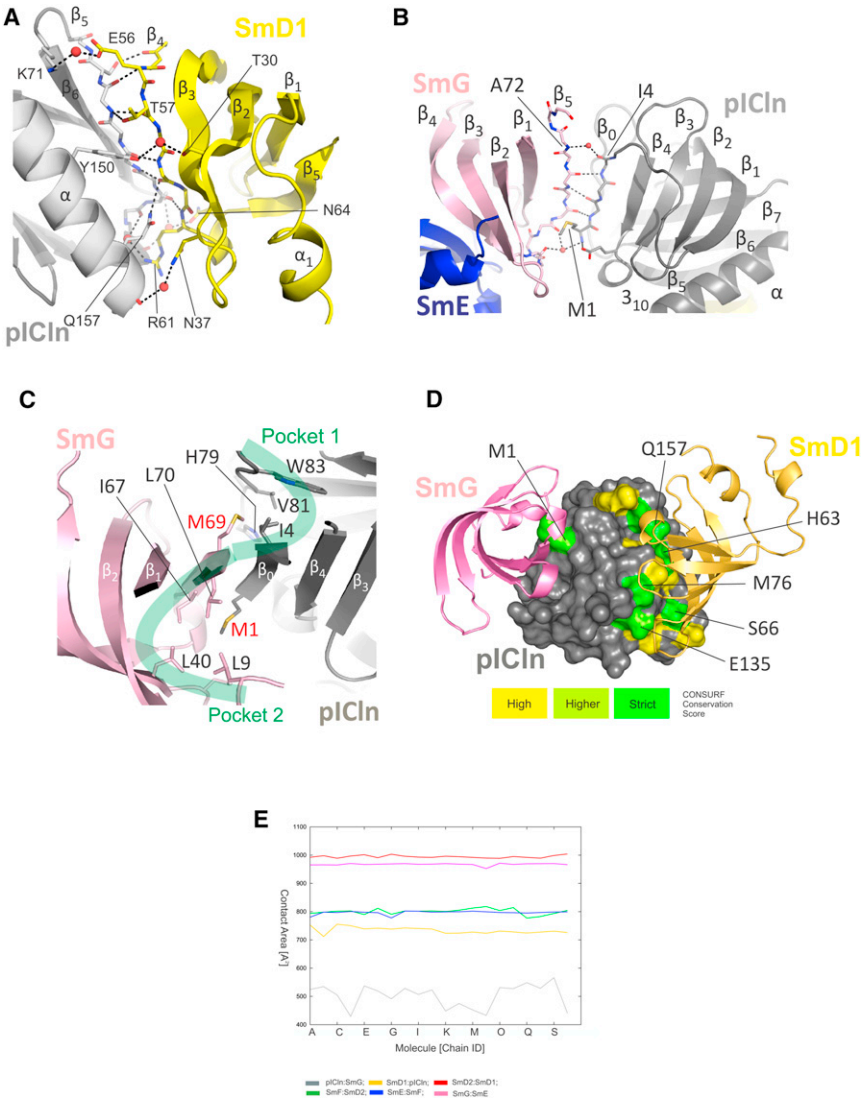

Figure 4. Detailed Representation of the pICln-SmD1 and the pICln-SmG Interface

(A) Interface of pICln with SmD1. β5 of pICln and β4 of SmD1 involved in β sheet formation are shown in stick representation, H bonds are shown as dashed lines, and three water molecules involved in water-mediated H bonds are shown as red spheres. Residues forming intersubunit H bonds via their individual side chains are labeled. See the Supplemental Information for an in-depth description and a supplemental description to this figure.

(B) Contacts between pICln and SmG comprising backbone-backbone interactions. The parallel β pair formed by strands β5 of SmG and β0 of pICln is shown in stick representation. H bonds are shown as dashed lines, two water molecules that mediate intersubunit contacts via H bonds are shown as red spheres. Residues mentioned in the text are labeled. pICln Met1 is shown in stick representation.

(C) Hydrophobic interactions between pICln and SmG. The location of the two pockets is indicated by green lines. Hydrophobic amino acids lining out the pockets are labeled as well as the two methionine residues bound within each pocket.

(D) Residues conserved among a variety of species, mapped onto the molecular surface of pICln. The underlying multiple sequence alignment is depicted in Figure S4.

(E) Contact area of the respective interfaces within the pICln/Sm ring of the 8S structure plotted for each of the 20 molecules of the asymmetric unit. See also Figure S4.

complex structures (Figure 5C). In good accordance with the findings from the 20 molecules in the crystal structure, the analysis of the resulting trajectories indicates that (1) the 8S complex features increased dynamic ("breathing") motions compared to 6S, (2) the SmG-pICln contact is the most flexible within the ring in both the 6S and the 8S complex, (3) in the 8S complex, this local increase in flexibility is significantly enhanced compared to the 6S complex, and, finally, (4) a preferred movement perpendicular to the ring plane that mirrors the one shown in Figure 5B for the 20 molecules of the asymmetric unit (data not shown).

Taken together, the observed intrinsic flexibility of 8S points to a predetermined site where pICln dissociation from the 6S ring is likely to be initiated and the means by which it is ultimately evicted. However, additional conformational changes, most probably induced by SMN's C terminus and/or other SMN complex subunits, must occur as pICln is still stably bound in the 8S complex.

pICln Release by the SMN Complex Activates Sm Proteins for snRNP Assembly

Our structural analysis of the 6S and 8S assembly intermediates suggests that displacement of pICln alone is necessary and sufficient for Sm protein transfer onto snRNA. To test this model by biochemical means, we performed snRNP assembly assays in vitro with 6S and 8S complexes and an additional complex that is equivalent to 8S but lacks pICln (termed 7S) (Chari et al., 2008). These complexes were incubated with radiolabeled U1snRNA or a mutant lacking the Sm site (U1ΔSm snRNA) and Sm subcore formation was monitored by native gel electrophoresis. Both reconstituted 6S and 8S complexes were inactive in snRNP assembly, confirming the kinetic trap imposed on Sm proteins in their pICln bound state (Figure 6, lanes 3 and 5, respectively). However, efficient formation of Sm subcores was observed when U1 snRNA was incubated with the 7S complex (Figure 6, lane 2). This reaction was strictly dependent on the presence of an Sm site (Figure 6, lane 9) and occurred with similar efficiency as the spontaneous assembly without assembly factors (Figure 6, lane 7). In striking contrast, preincubation of the 7S complex with an equimolar amount of pICln reduced Sm subcore formation by nearly 65% (Figure 6, lane 4). The conclusions of these experiments are

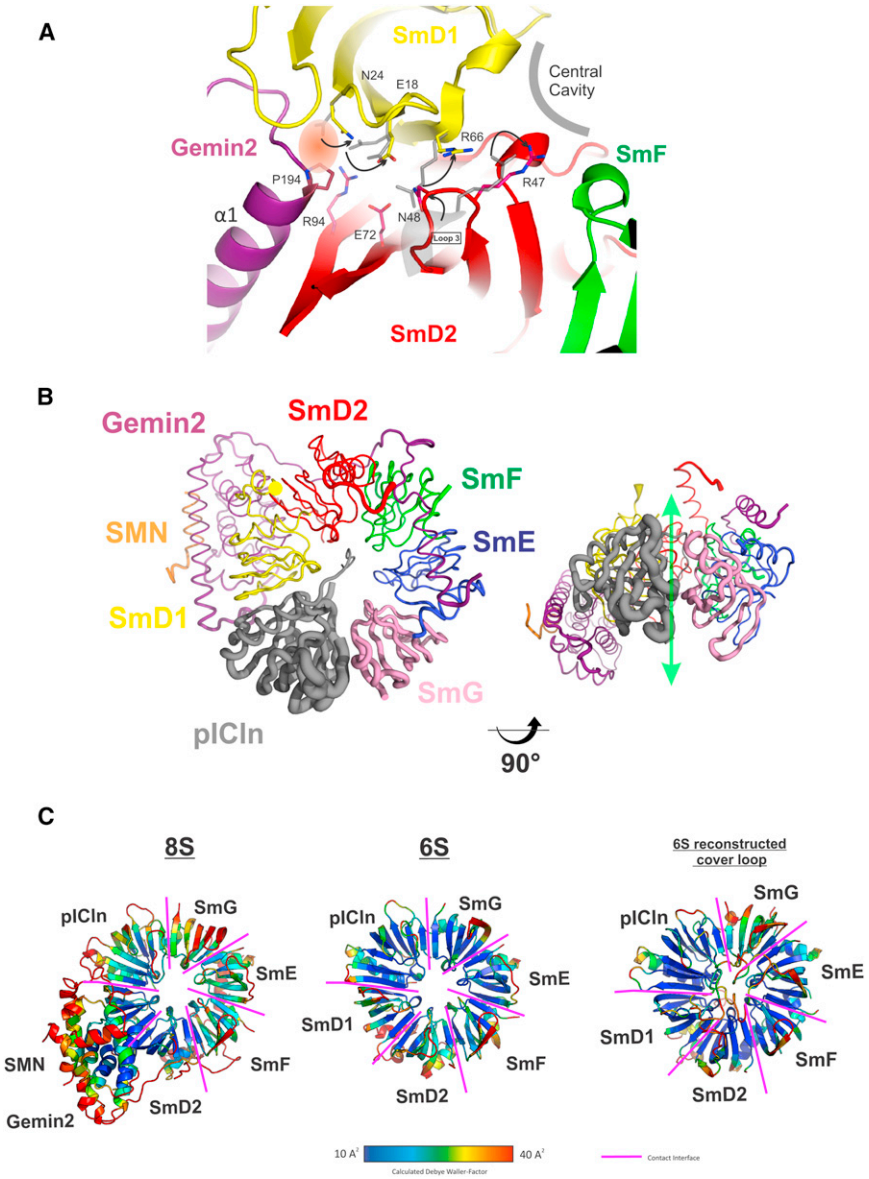

Figure 5. Molecular Flexibility of the 8S Complex

(A) Overlay of the 8S model (colored) with the 6S model (transparent, gray) viewed in the Gemin2 contact region. Arrows indicate the conformational changes induced by Gemin2 binding. The conformations seen in 6S would produce a clash upon Gemin2 binding (red ellipse).

(B) Tube representation of the 8S complex. The tube diameter is proportional to the rmsd values of the respective Cα positions among the 20 molecules within the asymmetric unit. The left view is shown from the flat face; the right view is turned 90°, and the green arrow indicates the main direction of positional deviation.

(C) Debye Waller ("temperature") factors calculated from three molecular dynamics trajectories simulated at 310K. Under equilibrium conditions, Debye-Waller factors were calculated from the coordinate differences of 1,500 states (corresponding to 3 ns simulation time) at the end of the trajectory. Sm β-β contacts are marked in pink. The 8S complex (left) features increased breathing motions mirrored by elevated temperature factors as compared to the 6S complex (middle). Note that the 8S pICln-SmG β-β contact features the highest temperature factors of all six transsubunit β-β contacts in the ring. A similar situation is found in 6S. However, the differences within the ring are less pronounced and the overall mobility of the molecule is lower. When the full cover loop of pICln and the crystallographcally invisible L2 loop of SmD2 were modeled and included in the simulation, a slight increase in mobility is visible for SmG and a slight decrease for SmD2 (right).

See also Figure S5, Table S1, and Movie S1.

derived from the quantification of three independent experiments, which are highly reproducible (Figure 6, bottom panel). These experiments, which receive full support by the structures presented in this study, indicate that the 7S complex represents an assembly competent state. Furthermore, they show that inhibition of snRNP assembly correlates with the formation of a closed-ring structure in 6S and 8S complexes by the binding of pICln to SmD1/D2 and SmE/F/G (Figures 1 and 2).

DISCUSSION

In this study we have solved the crystal structures of two key intermediates of snRNP assembly. Along with the structure of the late assembly intermediate, a glimpse into the mode of action of the assembly machinery at atomic resolution is now obtained (Figure 7).

The 6S complex represents a key in vivo reaction intermediate in the early phase of snRNP assembly. It is formed after Sm proteins have been sequestered and methylated by the PRMT5 complex and is released from the latter as a separate particle. Formation of this first higher-order assembly of the hetero-oligomers SmD1/D2 and SmE/F/G, however, occurs at the expense of a kinetic trap. The 1.9 Å structure of the 6S complex provides a conclusive explanation for how pICln knits this Sm hetero-oligomer into a complex that is incapable of forming in the absence of snRNA (Raker et al., 1996). An NMR study had elucidated that canine pICln contains a PH-like domain (Fürst et al., 2005), which is confirmed by our study (Figure 1B). However, the crystal structure of pICln reveals that the PH fold topology is extended in the 6S complex by an additional eighth β strand (β0, see Figure 1B), which was disordered in the NMR structure. We had previously demonstrated that pICln forms a stable complex with SmD1/D2 but is incapable of a direct interaction with SmE/F/G (Chari et al., 2008). Consequently, it appears that this β0 strand only becomes ordered upon formation of the 6S complex. By the help of this appendage, the extended PH fold

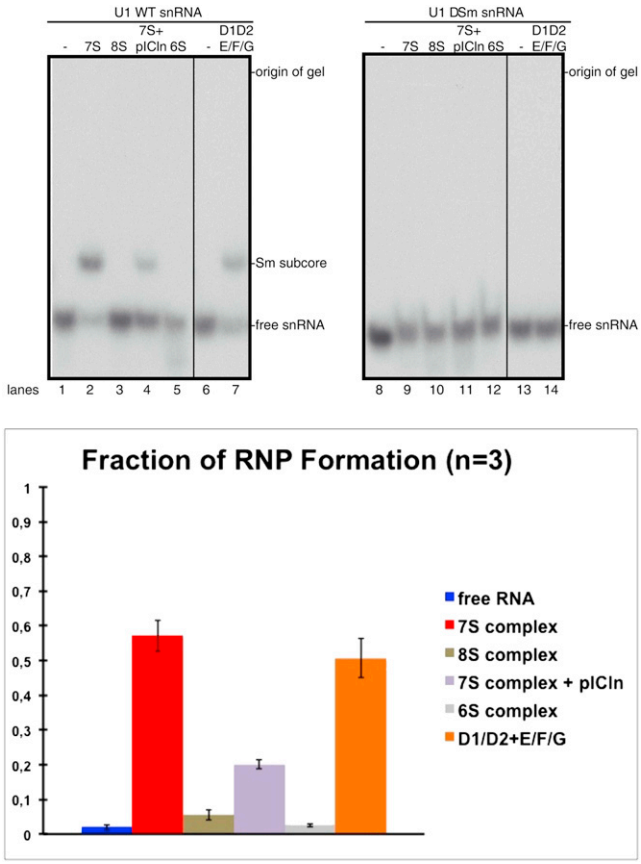

Figure 6. In Vitro Assembly of U1 snRNP with Key Assembly Intermediates

Assembly reactions with [32P]-labeled wild-type U1 snRNA and a mutant lacking a functional Sm site (U1ΔSm snRNA) were resolved by native gel electrophoresis. Shown are the respective RNAs alone (lanes 1, 6, 8, and 13), incubated with the 7S complex (lanes 2 and 9), the 8S complex (lanes 3 and 10), the 7S complex preincubated with an equimolar amount of pICln (lanes 4 and 11), the 6S complex (lanes 5 and 12), and isolated SmD1/D2 and SmE/F/G (lanes 7 and 14). Note that the 7S complex forms an Sm subcore complex with similar efficiency as the isolated Sm protein heterooligomers (lanes 2 and 7, with an average efficiency of 57 and 50%, respectively). This reaction is strictly dependent on a functional Sm site (compare lanes 2 and 7 with lanes 9 and 14, respectively). The preincubation of the 7S complex with an equimolar amount of pICln reduces its assembly activity by approximately 65% (compare lanes 2 and 4; with an average efficiency of 20%). In the bottom panel the densitometric quantification of three independent band shift experiments is depicted. The SD of three experiments is shown as error bars.

of pICln fits into the spatial gap that is occupied by SmD3/B in the mature snRNP. This molecular mimicry of a canonical Sm protein allows the imitation of an Sm-Sm interaction mode in its binding interfaces. Interestingly, pICln occupies an angular space of only 1 ½ Sm proteins within the 6S torus and thus forms a ring that is considerably narrower than that of the assembled Sm core domain (Figure 1C). Moreover, an electrostatic steering mechanism, driven by the ideally aligned dipole moment of the assembly chaperone (Figure 1D, lower left image), is likely to dominate an early interaction phase with Sm proteins. Additionally, the pronounced charge complementarity between the chaperone and its client proteins (Figure 1D) may contribute to the stability of the 6S complex under steady-state conditions. This view finds support in the evolutionary overall low sequence conservation of pICln, while its calculated pI values are unexpectedly constant, ranging from 3.8 to 4.2 (Figure S4). It is therefore likely that the pronounced negative charge on the molecular surface of pICln, rather than its amino acid sequence represents a conserved feature, which is essential to sustain the pICln-imposed kinetic trap in the 6S complex.

The crystal structures of U1 and U4 snRNPs have indicated that the seven Sm proteins occupy distinct and noninterchangeable positions in the assembled Sm core domain. Remarkably, the five Sm proteins D1, D2, E, F, and G are spatially arranged in the same sequential order within the 6S complex (Figures 1A and 1C). pICln's specific contact to SmD1 determines this order (Figure 4A), which is preserved in the 8S complex (Figure 2A), as well as in the late assembly intermediate. In contrast, an analogous contact of pICln to the SmF subunit of the SmE/F/G heterotrimer, which would change the order of Sm proteins in the 6S complex and consequently also in the Sm core cannot form for sterical reasons (Figure S1). Therefore, pICln constitutes a topological organizer that determines the positions of Sm proteins in the mature Sm core particle already at an early stage of assembly.

There are no obvious sequence homologs of pICln in the database. Nevertheless, the structural principles of its mode of action strikingly resemble those of other assembly chaperones, such as that of the Rubisco holoenzyme RbcX as well as of replication-dependent histone chaperones. These principles entail the binding of client proteins at positions, which are involved in the formation of higher-order structures of the final assembly at the expense of the formation of a kinetic trap (Chari and Fischer, 2010).

The SMN complex accepts preassembled Sm proteins from the assembly chaperone pICln and enables their transfer onto target snRNA. Although the SMN complex of vertebrates is composed of nine subunits, SMN and Gemin2 are sufficient for key aspects of snRNP assembly and are widely conserved among metazoan species (Kroiss et al., 2008). We hence focused on the structure elucidation of a trapped assembly intermediate that represents the "handover" of Sm proteins from the 6S complex onto a minimal SMN complex. This 8S intermediate is stalled due to the lack of the SMN C terminus (Chari et al., 2008). Our 8S model displays an rmsd of only 1.6 Å to the structure of the late assembly intermediate solved by Zhang et al. (2011) (see Table S1). The latter consists of Gemin2 bound to a small N-terminal peptide of SMN and the Sm proteins D1, D2, E, F, and G and represents an assembly stage, where pICln has already been released. In both complexes only a single helix of SMN is visible (Figure 2; Zhang et al., 2011). However, our 8S complex contained additional parts of SMN including the Tudor domain, which binds the sDMA-modified tails of SmB/B′, SmD1 and SmD3 (Friesen et al., 2001a; Tripsianes et al., 2011). Likewise, the putatively mobile and highly acidic cover loop of pICln was present in the crystallized construct but could not be located in the electron density (Figures 1D and S4). Both elements could be positioned by our EM reconstruction to the tapered face of the pICln/Sm ring (Figure 3). Surprisingly, the exit point of the SmD1 tail lies on the opposing flat face, from where Gemin2 would

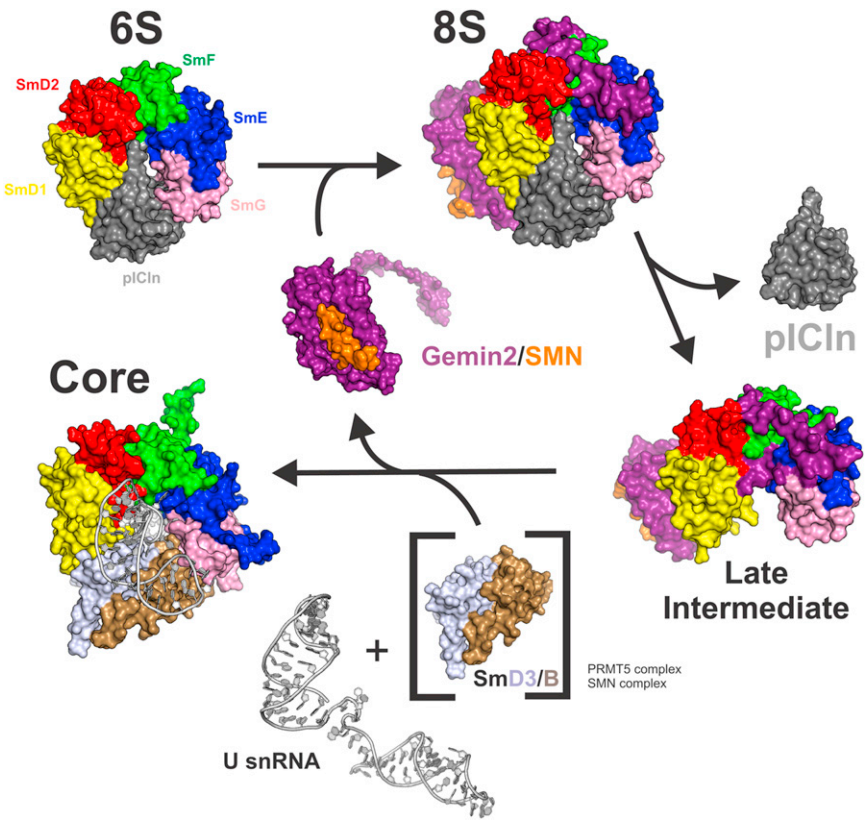

Figure 7. Structure-Based Schematic Representation of the snRNP Assembly Reaction

The 6S and 8S structures are from this report, the structure of the late assembly intermediate (PDB ID code 3S6N) has been described by Zhang et al. (2011) and structures of the assembled Sm core have been described by Leung et al. (2011), Weber et al. (2010), and Pomeranz Krummel et al. (2009) (PDB entry 2Y9A was used to produce the figure). See also Movie S1.

obstruct an interaction with the SMN Tudor domain. It is therefore unlikely that the sDMA-Tudor interaction plays a role in the stable binding of the heterooligomers SmD1/D2 and SmE/F/G to the SMN-complex. However, this does not rule out a possible relevance at other stages of the assisted assembly reaction. The structural analysis of intermediates containing additional components, like the full-length SMN-protein and SmD3/B will help to clarify this issue.

A comparison of our 8S model with the structure of the late assembly intermediate uncovered functionally important differences. While gross structural features of Gemin2 and its mode of interaction to the N terminus of SMN are very similar (Figure 2; see Figure S2 for a superposition of the SMN/Gemin2 units from both structures) differences can be identified for residues N-terminal to Gemin2's α1 helix (amino acids 1–29 of the fly and 1–46 of the human sequence). They were traced in the late assembly intermediate within the central cavity and had been suggested to inhibit snRNP formation (Zhang et al., 2011), whereas in the 8S complex this interaction is incompatible with the presence of the cover loop of pICln (Figure 3). However, in agreement with our prior findings (Chari et al., 2008) both 6S and 8S complexes represent assembly inactive states (Figure 6). In striking contrast, the 7S complex, which is equivalent to the late assembly intermediate but contains additional segments of SMN including the Tudor domain, was fully capable of transferring Sm proteins onto snRNA (Figure 6). Remarkably, preincubation of the 7S complex with isolated pICln suppressed its assembly activity. These findings are in accordance with pICln being inhibitory to snRNP formation and the 7S complex representing an assembly competent state. Thus, the details of mode and extent of snRNP assembly inhibition by the N-terminal residues of Gemin2 remains a subject of future studies. Notably, however, positioning of this part of Gemin2 in the snRNA binding site of SmD1/D2 and SmE/F/G might be essential to promote disassembly of preformed Sm subcores as reported and might contribute to a proofreading activity of the SMN complex (Chari et al., 2008; Kroiss et al., 2008; Pellizzoni et al., 2002).

How is the expansion of a six-membered 6S complex to a seven-membered ring in the assembled Sm core domain achieved? The structures of assembly intermediates presented in this study suggest a plausible solution to this puzzle. Analysis of the 20 conformers of the 8S complex (Figure 5B) and of MD trajectories (Figure 5C) reveals a pronounced structural flexibility around the pICln-SmG contact, thus suggesting the likely position where and providing a possible explanation for how pICln binding is destabilized. The distinct directionality of the observed movement perpendicular to the ring plane suggests that ring opening proceeds in the same direction. Obviously, distortion of the pICln/Sm ring is favored at the pICln-SmG interface due to its limited buried surface area (450–550 $Å^2$), which is considerably smaller than the areas of all other interfaces within the ring that range from 700 to 1,000 $Å^2$ (Figure 4E). This observation is in line with the observations from our MD simulation that clearly identify the pICln-SmG contact as a mobility hotspot of the ring (Figure 5C). The simulation also indicates that both the binding of SMN-Gemin2 as well as the pICln cover loop are factors that foster the intrinsic mobility at this position. More insight into the molecular basis of ring opening is obtained by measuring the distance of two marker atoms in SmD1 (Leu58, Cα) and SmG (Leu70, Cα). Their distance is gradually increased from 28.6 Å in 6S/8S complexes, to 30.7 Å in the late assembly intermediate and finally to 38.8 Å in assembled snRNP cores. A superimposition of these structures on SmD1/D2 reveals that a significant movement of SmG perpendicular to the ring plane occurs during the opening of the ring. Upon formation of the snRNP core domain by the binding of D3/B, SmG moves back

into the plane. Thus, the extraplanar distortion of Sm proteins observed in the late assembly intermediate appears to relax a strain, which is prevalent in the 6S/8S complexes, and enables ring expansion. It is noteworthy that this bears striking resemblance to the mode of action of clamp loading enzymes (Kelch et al., 2011) in the absence of any other compositional, functional and mechanistic similarities.

The SMN complex acts as a catalyst in the formation of snRNPs (Chari et al., 2008), but its molecular basis has remained elusive. The available structures now provide a plausible explanation for its catalytic activity. An opening of the pICln-SmG contact driven by the molecular motion of the 8S complex is expected to be transient. If, however, the SMN complex were to bind to such transiently exposed portions of the pICln-SmG contact surface and thus stabilize an open ring conformation, it would lower the energy barrier associated with the kinetic trap and thus provide rate acceleration. A likely candidate possessing a possible transition-state affinity is the Tudor domain of SMN (see Movie S1), which is an Sm fold mimic and lies, as we have shown by a combination of different techniques, in the vicinity of the predetermined breaking point (Figure 3B). Notably, such a means of rate acceleration has a precedent in donor strand exchange reactions performed by pilus chaperones in the assembly cycle of type1 pili of gram-negative bacteria (Nishiyama et al., 2008). The validation of this hypothesis and the potential contribution of other parts of the SMN complex, awaits further mechanistic and structural studies.

EXPERIMENTAL PROCEDURES

Detailed experimental procedures can be found in the Supplemental Experimental Procedures. A comprehensive report on the crystallographic structure determination will be published elsewhere.

Protein Expression, Complex Reconstitution, and Crystallographic Structure Determination

Human SmD1/D2, SmE/F/G, and fly SMN/Gemin2 complexes were co-expressed in *E. coli*. Fly pICln was expressed as a single protein. 6S and 8S complexes were reconstituted by mixing the respective subunits in presence of 1 M NaCl, followed by dialysis to 150 mM NaCl (see the Supplemental Experimental Procedures for a detailed description), the 7S complex was prepared as described (Chari et al., 2008). Crystals were grown by the hanging drop method and data collected on a synchrotron beamline. Diffraction-quality 6S crystals could only be obtained after introduction of particular point mutations and a deletion within the pICln cover loop. The 8S crystal structure was solved by molecular replacement with PDB entry 3S6N used as a search model. Refinement was done with NCS and reference model restraints with the high-resolution 6S model used as a reference structure. In the last refinement rounds, the NCS restraints were released for divergent parts of the model. The 6S crystal structure was solved by molecular replacement with the pICln/Sm ring from the 8S crystal structure used as a search model.

Native Gel Electrophoresis of RNA-Protein Complexes

Band shift assays were performed essentially as described (Chari et al., 2008). For the preincubation experiment with pICln, 3 pmol 7S complex was mixed with 3 pmol pICln in the presence of 10% glycerol, 0.1 U/μl RNAsin (Promega), 0.1 μg/μl tRNA and incubated at 4°C for 20 min prior to the addition of 0.3 pmol of radio-labeled RNA.

Electron Microscopy and Single-Particle Image Processing

The 8S complex was subjected to the GraFix method and stained with uranyl formate as previously described (Chari et al., 2008). Ten thousand single-particle images were selected and subjected to contrast transfer function (CTF) correction. With iteratively refined class averages, CTF-corrected single-particle images were aligned via an exhaustive polar alignment and subsequent multivariate statistical analysis-based hierarchical ascendant classification into classes of ≈20 members in average. We used the low-pass filtered X-ray structure of the 8S complex to assign initial angles to the class averages. The structure was determined by angular reconstitution and iteratively refined by several rounds of projection matching. The resulting structure had a resolution of 20 Å as determined by the Fourier shell correlation 0.5 σ criterion.

ACCESSION NUMBERS

The coordinates of the structures reported in this paper have been deposited in the Protein Data Bank under ID codes 4F7U (6S complex) and 4F77 (8S complex). The EM reconstruction has been deposited in the EMDB under ID code 2102.

SUPPLEMENTAL INFORMATION

Supplemental Information includes Supplemental Experimental Procedures, five figures, two tables, and one movie and can be found with this article online at http://dx.doi.org/10.1016/j.molcel.2012.12.009.

ACKNOWLEDGMENTS

We thank the staff of beamlines ID14-4, ID14-1, ID29, ID23-1, ID23-2, and BM16 (ESRF, Grenoble) and beamlines PX-II and PX-III (SLS,Villigen) and R. Kiefersauer (Proteros Biostructures) for their excellent support. Crystallization screening was carried out in part at the HT-X facility Grenoble within the SPINE framework. This work was supported by grants of the DFG to U.F. (FI 573/7-1) and to A.C. (CH 1098/1-1) and the RVZ (C.K., H.S., and U.F.).

Received: May 25, 2012
Revised: November 6, 2012
Accepted: December 13, 2012
Published: January 17, 2013

REFERENCES

Alberts, B. (1998). The cell as a collection of protein machines: preparing the next generation of molecular biologists. Cell *92*, 291–294.

Brahms, H., Meheus, L., de Brabandere, V., Fischer, U., and Lührmann, R. (2001). Symmetrical dimethylation of arginine residues in spliceosomal Sm protein B/B' and the Sm-like protein LSm4, and their interaction with the SMN protein. RNA *7*, 1531–1542.

Bühler, D., Raker, V., Lührmann, R., and Fischer, U. (1999). Essential role for the tudor domain of SMN in spliceosomal U snRNP assembly: implications for spinal muscular atrophy. Hum. Mol. Genet. *8*, 2351–2357.

Chari, A., and Fischer, U. (2010). Cellular strategies for the assembly of molecular machines. Trends Biochem. Sci. *35*, 676–683.

Chari, A., Golas, M.M., Klingenhäger, M., Neuenkirchen, N., Sander, B., Englbrecht, C., Sickmann, A., Stark, H., and Fischer, U. (2008). An assembly chaperone collaborates with the SMN complex to generate spliceosomal SnRNPs. Cell *135*, 497–509.

Chari, A., Paknia, E., and Fischer, U. (2009). The role of RNP biogenesis in spinal muscular atrophy. Curr. Opin. Cell Biol. *21*, 387–393.

Derewenda, Z.S., and Vekilov, P.G. (2006). Entropy and surface engineering in protein crystallization. Acta Crystallogr. D Biol. Crystallogr. *62*, 116–124.

Ellis, R.J. (2001). Macromolecular crowding: obvious but underappreciated. Trends Biochem. Sci. *26*, 597–604.

Ellis, R.J. (2006). Molecular chaperones: assisting assembly in addition to folding. Trends Biochem. Sci. *31*, 395–401.

Fischer, U., Englbrecht, C., and Chari, A. (2011). Biogenesis of spliceosomal small nuclear ribonucleoproteins. Wiley Interdiscip Rev RNA *2*, 718–731.

Fisher, D.E., Conner, G.E., Reeves, W.H., Wisniewolski, R., and Blobel, G. (1985). Small nuclear ribonucleoprotein particle assembly in vivo: demonstration of a 6S RNA-free core precursor and posttranslational modification. Cell *42*, 751–758.

Friesen, W.J., Massenet, S., Paushkin, S., Wyce, A., and Dreyfuss, G. (2001a). SMN, the product of the spinal muscular atrophy gene, binds preferentially to dimethylarginine-containing protein targets. Mol. Cell *7*, 1111–1117.

Friesen, W.J., Paushkin, S., Wyce, A., Massenet, S., Pesiridis, G.S., Van Duyne, G., Rappsilber, J., Mann, M., and Dreyfuss, G. (2001b). The methylosome, a 20S complex containing JBP1 and pICln, produces dimethylarginine-modified Sm proteins. Mol. Cell. Biol. *21*, 8289–8300.

Fürst, J., Schedlbauer, A., Gandini, R., Garavaglia, M.L., Saino, S., Gschwentner, M., Sarg, B., Lindner, H., Jakab, M., Ritter, M., et al. (2005). ICln159 folds into a pleckstrin homology domain-like structure. Interaction with kinases and the splicing factor LSm4. J. Biol. Chem. *280*, 31276–31282.

Gubitz, A.K., Feng, W., and Dreyfuss, G. (2004). The SMN complex. Exp. Cell Res. *296*, 51–56.

Hartwell, L.H., Hopfield, J.J., Leibler, S., and Murray, A.W. (1999). From molecular to modular cell biology. Nature *402*(6761, Suppl), C47–C52.

Kambach, C., Walke, S., Young, R., Avis, J.M., de la Fortelle, E., Raker, V.A., Lührmann, R., Li, J., and Nagai, K. (1999). Crystal structures of two Sm protein complexes and their implications for the assembly of the spliceosomal snRNPs. Cell *96*, 375–387.

Kastner, B., Fischer, N., Golas, M.M., Sander, B., Dube, P., Boehringer, D., Hartmuth, K., Deckert, J., Hauer, F., Wolf, E., et al. (2008). GraFix: sample preparation for single-particle electron cryomicroscopy. Nat. Methods *5*, 53–55.

Kelch, B.A., Makino, D.L., O'Donnell, M., and Kuriyan, J. (2011). How a DNA polymerase clamp loader opens a sliding clamp. Science *334*, 1675–1680.

Kroiss, M., Schultz, J., Wiesner, J., Chari, A., Sickmann, A., and Fischer, U. (2008). Evolution of an RNP assembly system: a minimal SMN complex facilitates formation of UsnRNPs in *Drosophila melanogaster*. Proc. Natl. Acad. Sci. USA *105*, 10045–10050.

Leung, A.K., Nagai, K., and Li, J. (2011). Structure of the spliceosomal U4 snRNP core domain and its implication for snRNP biogenesis. Nature *473*, 536–539.

Meister, G., Bühler, D., Pillai, R., Lottspeich, F., and Fischer, U. (2001a). A multiprotein complex mediates the ATP-dependent assembly of spliceosomal U snRNPs. Nat. Cell Biol. *3*, 945–949.

Meister, G., Eggert, C., Bühler, D., Brahms, H., Kambach, C., and Fischer, U. (2001b). Methylation of Sm proteins by a complex containing PRMT5 and the putative U snRNP assembly factor pICln. Curr. Biol. *11*, 1990–1994.

Nishiyama, M., Ishikawa, T., Rechsteiner, H., and Glockshuber, R. (2008). Reconstitution of pilus assembly reveals a bacterial outer membrane catalyst. Science *320*, 376–379.

Pellizzoni, L., Yong, J., and Dreyfuss, G. (2002). Essential role for the SMN complex in the specificity of snRNP assembly. Science *298*, 1775–1779.

Pomeranz Krummel, D.A., Oubridge, C., Leung, A.K., Li, J., and Nagai, K. (2009). Crystal structure of human spliceosomal U1 snRNP at 5.5 A resolution. Nature *458*, 475–480.

Raker, V.A., Plessel, G., and Lührmann, R. (1996). The snRNP core assembly pathway: identification of stable core protein heteromeric complexes and an snRNP subcore particle in vitro. EMBO J. *15*, 2256–2269.

Tarn, W.Y., and Steitz, J.A. (1997). Pre-mRNA splicing: the discovery of a new spliceosome doubles the challenge. Trends Biochem. Sci. *22*, 132–137.

Tripsianes, K., Madl, T., Machyna, M., Fessas, D., Englbrecht, C., Fischer, U., Neugebauer, K.M., and Sattler, M. (2011). Structural basis for dimethylarginine recognition by the Tudor domains of human SMN and SPF30 proteins. Nat. Struct. Mol. Biol. *18*, 1414–1420.

Wahl, M.C., Will, C.L., and Lührmann, R. (2009). The spliceosome: design principles of a dynamic RNP machine. Cell *136*, 701–718.

Weber, G., Trowitzsch, S., Kastner, B., Lührmann, R., and Wahl, M.C. (2010). Functional organization of the Sm core in the crystal structure of human U1 snRNP. EMBO J. *29*, 4172–4184.

Yong, J., Wan, L., and Dreyfuss, G. (2004). Why do cells need an assembly machine for RNA-protein complexes? Trends Cell Biol. *14*, 226–232.

Zhang, R., So, B.R., Li, P., Yong, J., Glisovic, T., Wan, L., and Dreyfuss, G. (2011). Structure of a key intermediate of the SMN complex reveals Gemin2's crucial function in snRNP assembly. Cell *146*, 384–395.